ISSN 2472-1972

An Excess of CYP24A1, Lack of CaSR, and a Novel lncRNA Near the PTH Gene Characterize an Ectopic PTH-Producing Tumor

Kosuke Uchida,[1,2] Yuji Tanaka,[2] Hitoshi Ichikawa,[3] Masato Watanabe,[4] Sachiyo Mitani,[3] Koji Morita,[5] Hiroko Fujii,[1,6] Mayumi Ishikawa,[7] Gen Yoshino,[8] Hiroko Okinaga,[5] Genta Nagae,[9] Hiroyuki Aburatani,[9] Yoshifumi Ikeda,[10] Takao Susa,[1] Mimi Tamamori-Adachi,[1] Toshio Fukusato,[4] Hiroshi Uozaki,[4] Tomoki Okazaki,[1] and Masayoshi Iizuka[1]

[1]Department of Biochemistry, Teikyo University School of Medicine, Tokyo 173-0003, Japan; [2]Department of General Practice, National Defense Medical College, Saitama 359-0042, Japan; [3]Genetics Division, National Cancer Center Research Institute, Tokyo 104-0045, Japan; [4]Department of Pathology, Teikyo University School of Medicine, Tokyo 173-0003, Japan; [5]Department of Internal Medicine, Teikyo University School of Medicine, Tokyo 173-0003, Japan; [6]Department of Internal Medicine, Self-Defense Forces Central Hospital, Tokyo 154-8532, Japan; [7]Diabetes and Arteriosclerosis, Nippon Medical School, Musashikosugi Hospital, Kanagawa 211-8533, Japan; [8]Center for Diabetes, Shinsuma General Hospital, Hyogo 654-0047, Japan; [9]Genome Science Laboratory Research Center for Advanced Science and Technology, The University of Tokyo, Tokyo 153-8904, Japan; and [10]Department of Surgery, Teikyo University School of Medicine, Tokyo 173-0003, Japan

Thus far, only 23 cases of the ectopic production of parathyroid hormone (PTH) have been reported. We have characterized the genome-wide transcription profile of an ectopic PTH-producing tumor originating from a retroperitoneal histiocytoma. We found that the calcium-sensing receptor (CaSR) was barely expressed in the tumor. Lack of CaSR, a crucial braking apparatus in the presence of both intraparathyroid and, probably, serendipitous PTH expression, might contribute strongly to the establishment and maintenance of the ectopic transcriptional activation of the PTH gene in nonparathyroid cells. Along with candidate drivers with a crucial frameshift mutation or copy number variation at specific chromosomal areas obtained from whole exome sequencing, we identified robust tumor-specific cytochrome P450 family 24 subfamily A member 1 (CYP24A1) overproduction, which was not observed in other non–PTH-expressing retroperitoneal histiocytoma and parathyroid adenoma samples. We then found a 2.5-kb noncoding RNA in the PTH 3′-downstream region that was exclusively present in the parathyroid adenoma and our tumor. Such a co-occurrence might act as another driver of ectopic PTH-producing tumorigenesis; both might release the control of PTH gene expression by shutting down the other branches of the safety system (*e.g.,* CaSR and the vitamin D3–vitamin D receptor axis).

Freeform/Key Words: PTH, ectopic production, lncRNA, calcium-sensing receptor, CYP24A1

Abbreviations: ATRX, α-thalassemia/mental retardation syndrome X-linked; CaSR, calcium-sensing receptor; cDNA, complementary DNA; CYP24A1, cytochrome P450 family 24 subfamily A member 1; DMEM, Dulbecco's modified Eagle medium; GAPDH, glyceraldehyde 3-phosphate dehydrogenase; HIC1, hypermethylated in cancer 1; iPTH, intact parathyroid hormone; lncRNA, long noncoding RNA; MFH, malignant fibrous histiocytoma; MFH+P, parathyroid hormone-producing malignant fibrous histiocytoma; PA, parathyroid adenoma; PBS, phosphate-buffered saline; PCR, polymerase chain reaction; PTH, parathyroid hormone; PTHrP, parathyroid hormone-related protein; qRT-PCR, quantitative real-time reverse transcription polymerase chain reaction; SNV, single nucleotide variation; VDR, vitamin D receptor; WBC, white blood cell.

Received 24 January 2017
Accepted 25 April 2017
First Published Online 3 May 2017

After birth, parathyroid hormone (PTH), produced in the parathyroid gland, regulates extracellular calcium, phosphate, and bone metabolism by replacing PTH-related protein (PTHrP), which has a similar function specifically in the fetal period. In contrast, humoral hypercalcemia of malignancy develops mostly by the robust reactivation of PTHrP production in adults when primary tumors acquire advanced aggressive characteristics [1, 2].

Paraneoplastic syndromes associated with malignant tumors, such as non–small lung cancers, are accompanied frequently by the ectopic production of peptide hormones [3]. However, the ectopic production of PTH, but not PTHrP, in malignancy is very rare, with merely 23 documented cases (Table 1). Accordingly, the etiology of ectopic PTH production remains elusive, except for a large gene rearrangement involving the PTH gene locus [4] or CpG hypomethylation of the PTH promoter [5]. We speculated that the parathyroid cell-specific expression of the PTH gene must be controlled extremely stringently and that escape from such restriction might be too difficult to permit PTH gene expression in nonparathyroid cells.

We report a case of hypercalcemia caused by ectopic PTH production in retroperitoneal malignant fibrous histiocytoma (MFH). We performed whole exome sequencing and used microarray profiling to identify molecular regulators that have the capability to induce PTH expression.

First, we examined the involvement of the deranged vitamin D axis. Inactivation of the active vitamin D3–vitamin D receptor (VDR) system is closely related to the tumorigenesis of various cancer cells [27–35]. Indeed, cytochrome P450 family 24 subfamily A member 1 (CYP24A1), an inactivating enzyme of active 1,25-dihydroxyvitamin D3, is considered a potent oncogene [33, 35].

We also explored the expression of hypermethylated in cancer 1 (HIC1), a tumor suppressor and potent CYP24A1 inducer [36–38]. We then explored the possible involvement of the expression of another potent brake candidate for PTH expression, namely, the calcium-sensing

Table 1. Ectopic PTH-Producing Tumors and Molecular Analyses

Patient Histopathologic Type	Detection of PTH RNA (Left) or Protein (Right)		Structural Alteration in PTH Gene	Reference
Small cell lung cancer	+	+		[6]
Clear cell ovarian adenoma	+	+	Rearrangement	[4]
Endometrial cancer		+		[7]
Neuroectodermal malignancy	+			[8]
Thymoma	+	+		[9]
Squamous cell lung cancer		+		[10]
Papillary thyroid cancer		+		[11]
Hepatocellular cancer				[12]
Squamous cell lung cancer		+		[13]
Small cell lung cancer	+	+		[14]
Ovarian neuroendocrine cancer		+		[15]
Small cell cancer of the ovary		+		[16]
Nasopharyngeal rhabdomyosarcoma	+			[17]
Pancreatic neuroendocrine cancer				[18]
Cervical paraganglioma		+		[19]
Hepatocellular cancer		+		[20]
Pancreatic neuroendocrine cancer	+	+	CpG hypomethylation	[5]
Papillary thyroid cancer		+		[21]
Medullary thyroid cancer	+			[22]
Thyrothymic ligament neuroendocrine tumor		+		[23]
Adrenal pheochromocytoma		+		[24]
Hepatocellular cancer				[25]
Gastric carcinoma		+		[26]
Retroperitoneal MFH	+	+	No mutations	Present study

receptor (CaSR), in this process. Lethal hypercalcemia has been induced by the systemic loss or mutation of the CaSR gene in mice and humans [39–41]. If any trigger serendipitously produces a tiny amount of PTH in certain nonparathyroid cells, its expression would then be increased by the ablation of CaSR and its intracellular signaling system in these cells. In addition, long noncoding RNAs (lncRNAs) are expressed in a markedly tissue-specific manner and are highly regulated during development and in response to physiological signals [42–44]. Thus, to identify other possible players in the process of tumorigenesis, we explored lncRNAs in the region surrounding the PTH gene in parathyroid adenoma (PA), PTH-producing MFH (MFH+P) samples, and other cultured cancer cells.

1. Materials and Methods

A. Samples, Cells, and Clinical Data

All samples were obtained after informed consent in accordance with protocols approved by the ethics committees at Teikyo University School of Medicine (approval no. 12-040), National Defense Medical College (approval no. 125), and the University of Tokyo (approval no. 2011–16). In addition to the patient's MFH, we analyzed PAs from two other unrelated patients from Teikyo University School of Medicine Hospital, and samples from either one or both were used in the corresponding experiments. All the patients' laboratory data were obtained from the Department of General Practice (K.U., Y. T.). The non–PTH-producing breast cancer cell lines MCF-7, MDA-MB-231, and T47D were purchased from American Type Culture Collection (Manassas, VA). HepG2 (hepatoma), LNCaP (prostate cancer), M059J (glioma), and H295R (adrenocortical cancer) cells were also from American Type Culture Collection. HaCaT (keratinocyte) cells were a gift from Dr. N. E. Fusenig at the Division of Differentiation and Carcinogenesis, German Cancer Research Center (Heidelberg, Germany). MT2 (T cell lymphoma), SKBR (breast cancer), and MDA-MB453 (breast cancer) cells were gifts from Dr. Shunji Takahashi at the Cancer Institute Hospital of the Japanese Foundation for Cancer Research. Rv22 (prostate cancer) cells were kindly provided by Dr. Shigeo Horie at Juntendo University Hospital.

B. PTH Histochemistry

For PTH protein staining, the resected MFH tumor was minced, submerged in Dulbecco's modified Eagle medium (DMEM), and incubated for 2 hours. The medium was assayed using a whole PTH assay kit (DS Pharma Biomedical, Osaka, Japan). For immunohistochemistry, formalin-fixed, paraffin-embedded sections were stained with mouse monoclonal anti-human PTH (1-34) anti-serum (AbD Serotec, Oxford, UK) using a VECTASTAIN Elite ABC kit (Vector Laboratories, Burlingame, CA). The primary anti-PTH antibody was used at concentrations of 1:1000, 1:250, 1:100, and 1:50, and the secondary antibodies were used at a concentration of 1:500. The MFH tumor was cultured in DMEM for 2 hours, followed by the measurement of whole PTH levels. A mock incubation medium served as the control.

C. Quantitative Real-Time Reverse Transcription Polymerase Chain Reaction Analysis

Oligonucleotide primers are listed in Supplemental Table 1. Total RNA isolated using RNAiso Plus (TaKaRa Biotechnology, Shiga, Japan) was reverse transcribed by priming with random hexamers and an oligo(dT) primer (PrimeScript RT reagent kit; TaKaRa Biotechnology, Shiga, Japan) or an oligo(dT) primer alone. Unless stated otherwise, all complementary DNAs (cDNAs) were obtained using a PrimeScript RT reagent kit with genomic DNA Eraser (TaKaRa Biotechnology). In the MFH, because the sample volume was limited, the absence of genomic DNA in the sample was verified using reverse transcription-free procedures or several unrelated intergenic and nonexonic primers as negative controls.

Quantitative real-time reverse transcription polymerase chain reaction (qRT-PCR) analysis was performed using a Thermal Cycler Dice TM TP860 and SYBR Premix

EXTaqII (TaKaRa Biotechnology). Samples were run in triplicate, unless stated otherwise. IBM SPSS Statistics, version 21, software (IBM Corp., Armonk, NY) was used for statistical analysis. We used one or two PAs from the patients, the MFH+P sample, and various cultured cancer cells. In some experiments, one to four non–PTH-producing MFH samples other than the MFH+P were included. For CaSR, VDR, and CYP24A1 amplification in the qRT-PCR assays, two sets of each primer (denoted −a and −b) were used.

D. DNA Sequencing

We synthesized PTH cDNA from RNA that was reverse transcribed with an oligo(dT) primer (TaKaRa Biotechnology), amplified a 697-bp cDNA product (coding capacity, between the 61st and 408th nucleotides) and cloned it into the pBluescript II SK(+) vector (Agilent Technologies, Santa Clara, CA). Two independent clones were sequenced on both strands. Genomic DNA was extracted from the MFH+P sample and the patients' leukocytes using the Wizard SV Genomic DNA Purification System (Promega, Madison, WI) and a QIAamp DNA Mini kit (QIAGEN, Hilden, Germany), respectively. To sequence the promoter region, nine overlapping DNA fragments (approximately 800 bp in size), covering a region from 5.7 kbp upstream to 360 bp downstream of the transcription start site, were amplified using PCR. This region was cloned into the pBluescript II SK(+) vector, and two to four independent clones were sequenced on both strands. PTH promoter genomic DNA from the tumor was converted with bisulfite using a MethylEasy Xceed Rapid DNA Bisulphite Modification Kit (Human Genetic Signatures, Sydney, Australia). A 232-bp fragment corresponding to −1312 to −1081 bp from the transcription start site, which contains two CpG sites, was amplified by PCR and cloned into the pGEM-T Easy vector (Promega, Madison, WI). Nine clones from the tumor and three clones from the PA were sequenced on both strands.

E. Gene Expression Profiling

The patient's MFH+P sample with his white blood cells (WBCs) as controls were used, and total RNA was extracted and labeled with biotin. Ten micrograms of biotin-labeled commentary RNA was hybridized to gene-specific probes on the Human Genome U133 Plus 2.0 Array according to the GeneChip 3′IVT Express Kit User Manual (Affymetrix, Santa Clara, CA). The signal level of each transcript was calculated using Affymetrix GeneChip Command Console software (Affymetrix, Santa Clara, CA). Microarray results were compared with those of four non–PTH-producing cases (GSM149191, GSM149193, GSM149194, and GSM149200) of MFH registered with Gene Expression Omnibus as GSE6481 [45]. Because the scaling of the microarray data matched that of GSE6481, the data were normalized such that the trim average of the signal level became 100 (MAS 5.0 algorithm). Probe set identifications that were common in the Affymetrix Human Genome U133A Array of GSE6481 were extracted. For an obtained transcript, an expression ratio based on Log2(non–PTH-producing/PTH-producing) was calculated. The probe sets showing an expression ratio that increased by more than twofold or decreased by more than one-half in the MFH+P compared with any of the other four MFHs were extracted, forming two groups of upregulated and downregulated gene sets, respectively. For each single gene in each group, based on the National Center for Biotechnology Information Entrez Gene identification, gene ontology terms were assigned. The frequency of gene ontology terms in a group was calculated, and their statistical significance (*P* value) was examined (TaKaRa Biotechnology).

F. Immunofluorescence

Specimens were collected at surgery from the patients. The patients' tissue samples were embedded in Tissue-Tek O.C.T. Compound (Sakura Finetek Japan, Tokyo, Japan) in liquid nitrogen. Tissue sections (6 to 7 μm) were cut using a cryomicrotome (CM3050S; Leica

Microsystems, Nussloch, Germany) at −21°C. For fixation, the samples were incubated in 4% paraformaldehyde in phosphate-buffered saline (PBS) for 20 minutes at room temperature.

Permeabilization was performed with 0.25% Triton X-100 in PBS for 20 minutes at room temperature. Nonspecific binding was blocked by incubation in 3% bovine serum albumin and 0.1% Triton X-100 in PBS for 1 hour at room temperature. The antibodies were diluted in this blocking solution at the indicated concentrations and incubated for 2 hours at room temperature. Secondary antibodies were also diluted in the blocking solution and incubated for 1 hour at room temperature. Nuclei were stained with 2 μg/mL 496-diamidine-29-phenylindole dihydrochloride (Roche, Mannheim, Germany) in PBS for 15 minutes at room temperature. Images were acquired using a laser-scanning confocal image system (A1R-A1 Confocal Microscope System; Nikon, Tokyo, Japan). The primary anti-CYP24A1, anti-VDR, and anti-CaSR antibodies were used at concentrations of 1:50, 1:100, and 1:50, respectively, and secondary antibodies were used at a concentration of 1:500 [46]. The following antibodies were used in the immunofluorescence analysis: anti-human CYP24A1 rabbit polyclonal antibody (H-87; catalog no. sc-66851; Santa Cruz Biotechnology, Santa Cruz, CA); antihuman VDR (D2K6W) rabbit monoclonal antibody (catalog no. 12550; Cell Signaling Technology, Danvers, MA); and anti-human CaSR mouse monoclonal antibody (5C10, ADD; ab19347; Abcam, Cambridge, UK). The secondary antibodies were Alexa Fluor 647 goat anti-mouse/rabbit IgG (H+L) (A-21236/A-21245; Molecular Probes, Eugene, OR).

G. RT-PCR for Longer cDNA Fragments and Identification of lncRNAs

RNAs whose quality was strictly verified as described were analyzed to identify lncRNAs that were expressed exclusively in the MFH+P tumor. Various RNAs in the cultured cells, MFH+P, and PAs, which were transcribed from approximately 50-kb regions of the PTH gene, including its 3′-flanking region, were used. For the initial shotgun real-time RT-PCR analyses, parts of candidate lncRNAs were amplified using >40 sets of randomly chosen, but PCR-suitable, primers. Subsequently, amplification of candidate lncRNAs was performed using each primer pair covering 1 to 5 kb, with a denaturation step at 94°C for 2 minutes, followed by 37 cycles of denaturation at 95°C for 10 seconds, primer annealing at 65°C for 30 seconds, and primer extension at 68°C for 3.5 minutes in a reaction volume of 50 μL using the KOD FX Neo polymerase system (Toyobo, Osaka, Japan). The reaction samples were stored at 4°C. Detection was performed with 0.9% agarose gel electrophoresis. The results of qRT-PCR for glyceraldehyde 3-phosphate dehydrogenase (GAPDH) or β-actin were used as a control. To examine the lncRNAs, either oligo(dT)- or random primer-derived RNAs from the PA, MFH+P, and various cultured cells were obtained. Finally, publicly open databases for whole genome RNA sequencing were reviewed to examine whether the lncRNAs found were registered in any of the databases. The presence of RNA in all samples, even when no lncRNA was amplified, was confirmed by the presence of GAPDH messenger RNA (mRNA). Samples obtained during the RNA extraction step still containing both genomic DNA and RNA were used to prove the validity of the primers

H. Exome Capture, Library Construction, and Sequencing

One microgram of DNA per sample was sheared using a Covaris SS Ultrasonicator (Covaris Inc., Woburn, MA). We used a Sciclone NGS workstation (Caliper Life Sciences, Hopkinton, MA) for automated library construction. Exome capture was performed using an Agilent SureSelect Human All Exon Kit, version 4 (Agilent Technologies). Each sample was sequenced on an Illumina HiSEquation 2000 instrument using a read length of 2 × 100 bp. Image analysis and base calling were performed using the Illumina pipeline with default settings.

I. Exome Sequence Processing

Burrows-Wheeler Aligner and NovoAlign software were used to align the sequence reads to the human reference genome (GRCh37/hg19). After removal of PCR duplicates, we used SRMA33 to improve variant discovery through local realignments of short-read next-generation sequencing

data. Tumor cellularity was estimated from an allelic imbalance in the matched tumor and normal samples (patient's WBCs) with a program examining the allelic fractions of heterozygous single nucleotide polymorphisms in regions with a loss of heterozygosity using an algorithm similar to that described previously [47]. Consequently, somatic mutant allele frequencies ≥15%, adjusted by the estimated tumor content ratios, were retained. Artifacts originating from errors in the sequence and mapping were also filtered out by checking the single nucleotide variation (SNV) positions and base quality scores for the supporting reads. Fisher's exact test was then used, and SNV candidates with $P > 0.2$ were removed. To eliminate germline variations in the present study, we performed comparative analyses using paired tumor and WBC samples from the same patient and extracted the somatic events detected only in tumor tissues. SNVs were annotated using ANNOVAR, version 36.

2. Results

A. Case Report

A 69-year-old man with dehydration was admitted to the National Defense Medical College Hospital for the investigation of severe hypercalcemia. Laboratory data on admission (Table 2) revealed that the corrected serum calcium level was 18.2 mg/dL, serum intact PTH (iPTH) was 532 pg/mL, PTHrP was <1 pmol/L, and serum 1,25-dihydroxyvitamin D3 was 6.8 pg/mL.

Hypercalcemia with elevated serum iPTH suggested primary hyperparathyroidism; however, we failed to detect any evidence for hyperparathyroidism on standard image analyses. The magnetic resonance imaging findings indicated a retroperitoneal tumor [Fig. 1(a)]. Treatment with fluid replacement, zoledronic acid, and elcatonin lowered the serum calcium level. However, shortly thereafter, the tumor became enlarged, and the serum calcium level increased again despite intensive therapy. Whole body computed tomography and bone scintigraphy revealed no signs of metastasis, suggesting that the retroperitoneal tumor secreted PTH. The tumor was surgically resected. Pathologically, most tumor cells were spindle-shaped and the interspersed giant cells had large atypical nuclei [Fig. 1(b)]. The tumor was immunohistochemically positive for vimentin, CD34, smooth muscle actin, and cytokeratin (AE1/AE3) αS100 (partially). Therefore, we diagnosed an MFH. After tumor resection, the serum iPTH concentration decreased dramatically to 23 pg/mL and the serum calcium level normalized [Fig. 1(c)].

The whole PTH concentration in the supernatant of the tumor cultured in DMEM was 4830 pg/mL [reference range, 10 to 39; Fig. 1(d)], implying that the tumor cells produced PTH. After discharge, the serum iPTH and calcium levels have been normal for 6 years with no tumor recurrence.

Table 2. Laboratory Findings on Admission

Variable	Result	Reference Range
Albumin, g/dL	3.4	3.9–4.9
BUN, mg/dL	56	8.0–20.0
Creatinine, mg/dL	2.43	0.5–1.0
Sodium, mEq/L	126	135–149
Potassium, mEq/L	3.8	3.5–4.9
Chloride, mEq/L	94	96–108
Calcium, mg/dL	17.6	8.4–10.4
Phosphate, mg/dL	4.6	2.5–4.5
Magnesium, mg/dL	3.7	1.9–2.5
Intact PTH, pg/mL	532	10–65
PTHrP, pmol/L	<1.0	<1.0
1,25-Dihydroxyvitamin D3, pg/m	6.8	20–60

Abbreviation: BUN, blood urea nitrogen.

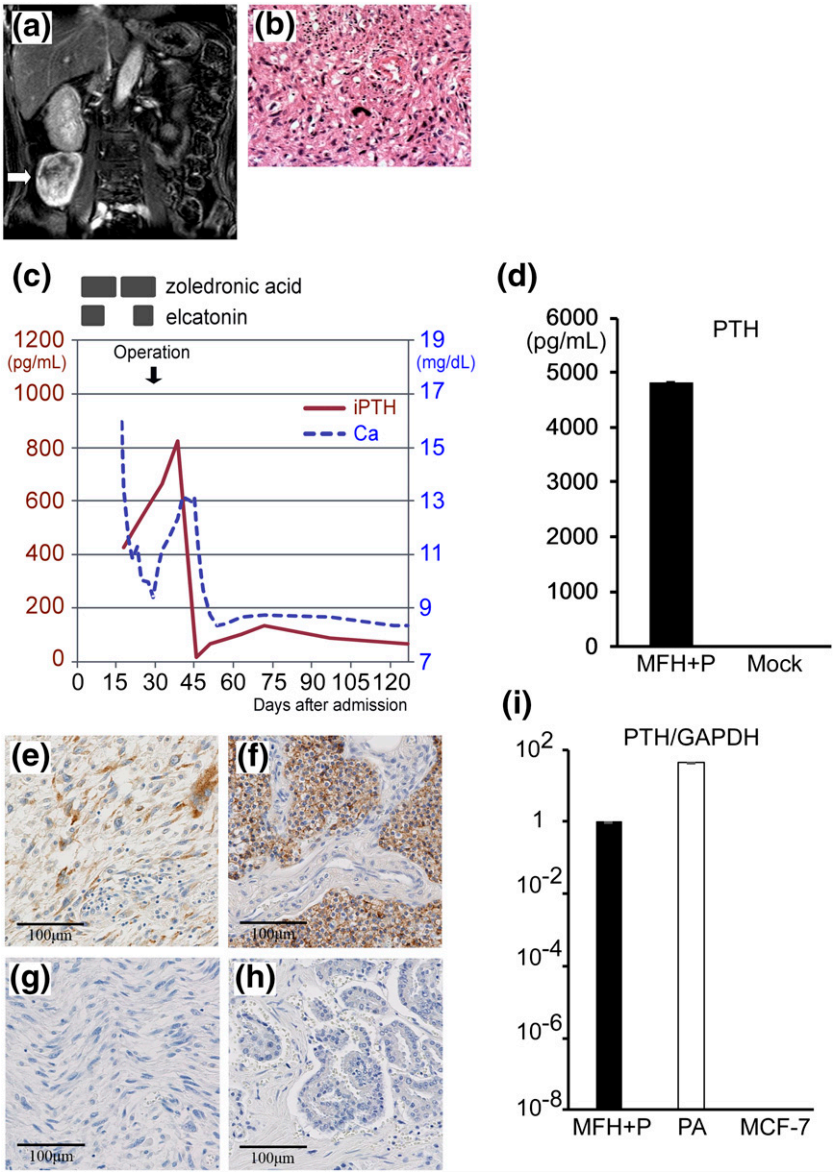

Figure 1. The MFH tumor and clinical course. (a) Enhanced coronal magnetic resonance image of the abdomen at hospitalization. An arrow indicates the retroperitoneal mass, 63 × 66 × 55 mm in size. (b) Hematoxylin and eosin staining of the retroperitoneal tumor (magnification, ×200). (c) Serum calcium and intact PTH levels in response to treatment with zoledronic acid, elcatonin, and tumor resection. (d) PTH expression in the MFH+P. The MFH+P tumor was cultured in DMEM for 2 hours, followed by measurement of whole PTH. A mock incubation medium served as a control. (e–h) Immunohistochemistry for PTH (magnification, ×200). (e) MFH+P tumor and (f) PA were stained with a mouse monoclonal anti-human PTH antibody. (g) MFH+P and (h) PA were stained with mouse IgG as negative controls. (i) qRT-PCR to assay the expression of PTH from the MFH+P and PA tumors and non–PTH-producing MCF-7 cells. The data were normalized by comparison with GAPDH expression.

B. PTH Expression in the Tumor

We examined PTH expression by immunohistochemistry. The tumor was stained with an anti-PTH antibody [Fig. 1(e)], similar to the PA [Fig. 1(f)]. Normal mouse IgG gave no signal [Fig. 1(g) and 1(h)]. We then measured the amount of PTH mRNA using qRT-PCR [Fig. 1(i)]. We used the PA as a positive control, and non–PTH-expressing MCF-7 cells were used as a

negative control. PTH mRNA expression was exceedingly high, comparable to that of the PA. PTHrP expression was not detected (data not shown).

C. Structural Analysis of the PTH Gene

To examine whether structural alteration of the PTH gene was responsible for the elevation [48], we examined PCR-amplified genomic regions of the PTH gene. We found neither any mutations in the coding and promoter sequences of the PTH gene nor hypomethylation of CpG dinucleotides in the PTH promoter (Supplemental Fig. 1). Sanger sequencing gave us consistent results. We did not find cyclin D overexpression in the MFH+P sample compared with four other non–PTH-producing MFHs or PA [49–51] (Fig. 2). Importantly, the 5′-flanking 5500-bp region of the PTH gene, which is necessary and sufficient to direct the parathyroid-specific expression of various transgenes in addition to the endogenous PTH gene [50, 52], contained no mutations.

D. Global Analysis of Gene Expression

We obtained the global expression profile of the MFH+P using microarray analyses (Fig. 3). As a control, we selected four non–PTH-producing MFHs, whose results we have made publicly accessible [45]. Of the four MFHs, one (termed GSM149194) originated from the retroperitoneum, similar to the MFH+P. As expected, PTH was one of the most highly activated genes (Fig. 3). Gene ontology analyses of the tumor (Supplemental Tables 2–5) revealed that molecules ensuring the spatiotemporal expression of genes only in the parathyroid environment [53–56] were not included in the MFH+P. The expression of the Gcm2 gene (Fig. 3), a master regulator of parathyroid gland development [56], was low in the MFH+P.

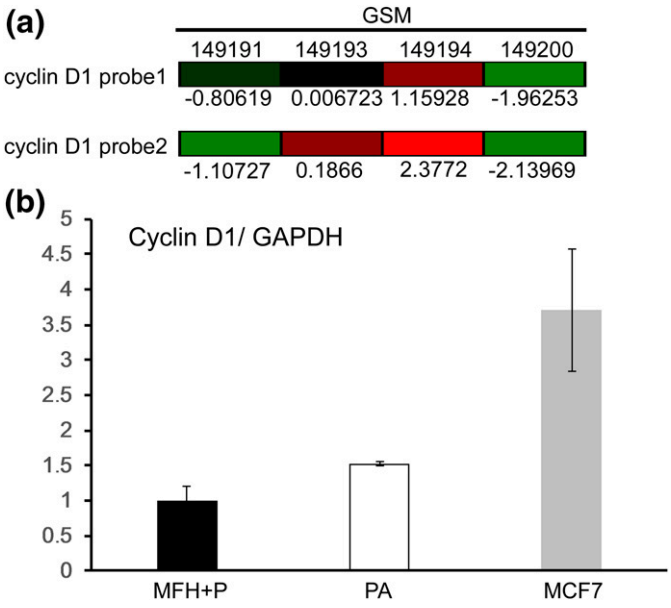

Figure 2. Cyclin D1 expression in the five MFHs (including the MFH+P), PA, and MCF-7 cells. (a) Comparison among the MFH+P and the four other MFHs (GSM149191, GSM14913, GSM149194, and GSM149200). Data were obtained from the registered microarray panel [45]. Green-to-red corresponds to elevated-to-reduced expression compared with that in the MFH+P. Two different probes were used. Numbers with a minus sign indicate an increase, and those without indicate a decrease in the mRNA level in MFH+P cells compared with each MFH (represented as an exponent of 2). (b) qRT-PCR of cyclin D1 mRNA from three cell types: MFH+P, PA, and MCF-7 breast cancer-cultured cells.

Furthermore, our subsequent qRT-PCR analysis using our MFH+P and the MFH GSM149194 revealed that the difference in the expression of PTH gene-related transcriptional and post-transcriptional factors was 2.5-fold at most between both (Supplemental Fig. 2) [48, 57–60].

Other candidates included redox factor 1 (apurinic/apyrimidinic endonuclease) and DNA-dependent protein kinase. We previously proposed that these two proteins were required for the extracellular calcium-dependent reduction of PTH mRNA [61–63]. We also wondered whether these proteins could function as negative regulators of the expression of certain genes in nonparathyroid cells [62]. Nonetheless, the expression levels of redox factor 1 and DNA-dependent protein kinase, and its regulatory subunits Ku70 and Ku86 were largely similar among the 5 MFHs and PA (Supplemental Fig. 3).

E. Whole Exome Sequencing

Whole exome sequencing revealed a frameshift mutation near the middle of the protein-coding region of the α-thalassemia/mental retardation syndrome X-linked (ATRX) gene and

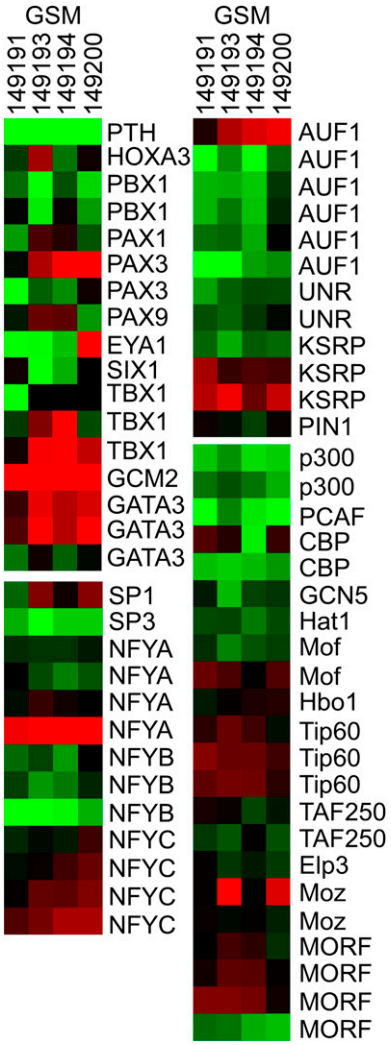

Figure 3. Transcriptional activation of the PTH gene through multiple mechanisms. A heatmap representing the expression levels of developmental genes for parathyroid genesis, transcriptional activators for PTH expression, proteins binding to PTH mRNA, and histone acetyltransferases in the MFH+P compared with those of the four other non–PTH-producing MFHs. Data were obtained from the registered microarray panel [45]. Green-to-red corresponds to elevated-to-reduced expression compared with that in MFH+P.

non–silent exonic mutations in 25 other genes [64–66] (Table 3). DNA from the patient's WBCs was used as a reference. The details of the analyses, including WBCs in the coding sequence in both samples, are shown in Supplemental Fig. 4. Because this gene is located on the X chromosome and its C-terminal portion has a crucial functional role as a tumor suppressor or chromosome modifier, our exome sequence analyses ruled out the possibility of an exon-breaking translocation with known genes (data not shown). In addition, we found >10 chromosomal copy number variations clustered at chromosome 11, where similar findings have been found in several PAs and hyperplasia (Table 4) [51, 67, 68].

F. CaSR and CYP24A1 Levels in the MFH+P Tumor

We next focused on molecules known to be specifically engaged in the regulation of PTH expression. We examined the expression of CaSR in five MFHs, including the MFH+P. CaSR mRNA was undetectable in all five MFH tumors, with little variance [Fig. 4(a)]. We then focused on the MFH+P by measuring CaSR mRNA levels using qRT-PCR. Compared with the PA, in which CaSR expression was robust, CaSR expression was almost undetectable in our MFH+P [Fig. 4(b)]. Dissociation curves after RT-PCR amplification [Fig. 4(c)] of MFH+P cDNA showed apparently bizarre shapes compared with the expected curves obtained from the PA, suggesting these were not primer dimers but indicating essentially no CaSR mRNA was expressed in the MFH+P. This was also the case for many other cultured cancer cells.

Another brake system for PTH expression is the 1,25-dihydroxyvitamin D3–VDR axis. Thus, we re-examined the expression of VDR in the MFH+P. The amount of VDR in the MFH+P was 1/20th of that in the PA [69]. The VDR cDNA levels in the other four MFH samples or cultured cancer cells varied [Fig. 4(a) and 4(d)]. Furthermore, qRT-PCR analysis of the MFH+P

Table 3. Whole Exome Sequencing of Paired MFH Tissues (MFH+P vs White Blood Cells)

Gene	Exonic Function	AA Change
USP24	Frameshift insertion	uc001cyg.4:c.5124_5125insT:p.I1708fs
PVRL4	Nonsynonymous SNV	uc010pjy.1:c.C311T:p.T104M
IPO9	Nonsynonymous SNV	uc001gwz.3:c.C1738T:p.L580F
DUSP10	Nonsynonymous SNV	uc001hmy.2:c.T463G:p.L155V
LRP2	Nonsynonymous SNV	uc002ues.3:c.C10416A:p.N3472K
TTN	Nonsynonymous SNV	uc021vtb.1:c.G67412A:p.S22471N
PGAP1	Nonsynonymous SNV	uc010fsi.3:c.T97C:p.Y33H
TBC1D19	Nonsynonymous SNV	uc011bxu.2:C1318T:p.L440F
RBM47	Nonsynonymous SNV	uc003gvd.2:c.G122A:p.R41H
RICTOR	Nonsynonymous SNV	uc003jlo.2:c.G2402T:p.G801V
PCDHA8	Nonsynonymous SNV	uc003lhr.1:c.G372T:p.K124N
UBR5	Nonsynonymous SNV	uc003ykr.2:c.G5227A:p.G1743S
LIPF	Nonsynonymous SNV	uc001kfg.2:c.T412C:p.W138R
MS4A6A	Nonsynonymous SNV	uc010rlb.2:c.T439G:p.C147G
BATF2	Nonsynonymous SNV	uc021qlb.1:c.C143T:p.A48V
DYNC2H1	Stopgain SNV	uc001pho.2:c.C12049T:p.Q4017X
CD163L1	Nonsynonymous SNV	uc001qsy.3:c.G4297T:p.G1433C
EEA1	Nonsynonymous SNV	uc001tck.3:c.G3228T:p.L1076F
ESRP2	Nonsynonymous SNV	uc002evq.1:c.G199C:p.V67L
MED1	Nonsynonymous SNV	uc010wee.2:c.C199T:p.P67S
FAM59A	Nonsynonymous SNV	uc002kxk.2:c.C2168T:p.A723V
RTTN	Nonsynonymous SNV	uc002lkp.2:c.G554A:p.R185K
ZNF335	Nonsynonymous SNV	uc010zxk.2:c.G1278A:p.M426I
ATRX[a]	Frameshift insertion	uc004ecq.4:c.3232_3233insT:p.S1078fs
GRIA3	Nonsynonymous SNV	uc004etq.4:c.C303G:p.I101M
GRIA3	Nonsynonymous SNV	uc004etq.4:c.C335T:p.T112I

Among 137 somatic mutations (123 SNVs, 14 indels), 39 exonic mutations, including 26 non-silent mutations (shown) were observed.

[a]ATRX with a frameshift mutation.

Table 4. Summary of Allelic Copy Number Variation (Both Gain and Loss)

Chromosome	Start	End	Copy Number	Gain/Loss	Number of Heterozygous SNPs
Chr2	41,686	49,215,977	1.0	Loss	1,094
Chr2	160,087,535	163,080,793	3.0	Gain	69
Chr2	166,894,230	169,020,166	3.0	Gain	36
Chr2	241,737,017	241,826,517	3.0	Gain	9
Chr2	241,826,754	242,265,313	4.0	Gain	77
Chr2	242,274,489	242,443,377	3.0	Gain	10
Chr3	12,616,533	13,679,335	3.0	Gain	38
Chr3	13,679,688	15,492,807	4.0	Gain	84
Chr3	15,507,761	16,280,076	3.0	Gain	31
Chr3	52,771,468	52,814,256	3.0	Gain	8
Chr3	52,815,905	54,615,971	4.0	Gain	52
Chr3	54,667,912	55,108,167	3.0	Gain	8
Chr4	40,337,908	44,704,938	3.0	Gain	69
Chr4	81,122,806	85,730,914	3.0	Gain	53
Chr4	142,155,214	143,236,158	3.0	Gain	9
Chr4	143,268,528	150,631,973	4.0	Gain	82
Chr4	150,632,186	152,049,296	3.0	Gain	13
Chr6	150,322,211	152,630,946	3.0	Gain	68
Chr7	154,680,910	157,232,668	3.0	Gain	107
Chr7	158,455,089	159,026,164	3.0	Gain	0
Chr9	107,586,753	111,635,101	3.0	Gain	65
Chr9	132,175,588	138,660,548	3.0	Gain	279
Chr9	140,507,688	141,071,552	3.0	Gain	0
Chr11	193,051	1,273,002	1.0	Loss	246
Chr11	1,272,245	5,565,906	3.0	Gain	244
Chr11	2,357,128	5,617,987	1.0	Loss	172
Chr11	5,573,024	6,737,979	4.0	Gain	62
Chr11	6,737,706	12,264,140	1.0	Loss	183
Chr11	6,738,291	17,491,571	3.0	Gain	252
Chr11	17,496,516	17,612,888	4.0	Gain	24
Chr11	17,612,972	26,700,099	3.0	Gain	172
Chr11	19,890,441	20,411,424	1.0	Loss	35
Chr11	26,718,692	33,075,917	4.0	Gain	64
Chr11	33,075,933	46,896,908	3.0	Gain	210
Chr11	33,778,729	41,830,789	1.0	Loss	94
Chr11	100,921,665	101,454,192	3.0	Gain	8
Chr11	101,762,478	102,736,642	4.0	Gain	59
Chr11	102,742,515	103,006,557	3.0	Gain	9
Chr12	57,030,026	57,109,931	3.0	Gain	8
Chr12	57,112,637	70,735,733	4.0	Gain	178
Chr12	70,740,194	70,930,061	3.0	Gain	7
Chr12	71,003,360	79,611,536	3.0	Gain	64
Chr13	32,915,413	36,822,849	3.0	Gain	70
Chr14	31,425,457	31,922,408	3.0	Gain	10
Chr14	32,047,217	36,400,983	4.0	Gain	45
Chr14	36,603,728	38,367,694	3.0	Gain	36
Chr14	38,368,184	45,432,870	4.0	Gain	46
Chr14	45,433,155	47,770,498	3.0	Gain	11
Chr15	66,641,956	72,143,855	3.0	Gain	125
Chr16	57,149,645	58,457,327	3.0	Gain	63
Chr18	12,976	3,075,778	3.0	Gain	94
Chr18	10,759,961	14,866,547	3.0	Gain	88
Chr18	32,487,955	50,912,352	3.0	Gain	136
Chr18	56,203,120	60,029,217	3.0	Gain	56
Chr19	308,662	6,677,989	3.0	Gain	484
Chr19	9,449,888	16,000,609	3.0	Gain	402
Chr19	16,006,101	16,976,289	4.0	Gain	60
Chr19	16,977,060	32,501,502	3.0	Gain	447

Table 4. Continued

Chromosome	Start	End	Copy Number	Gain/Loss	Number of Heterozygous SNPs
Chr19	41,198,482	41,415,818	3.0	Gain	46
Chr20	61,870,727	62,737,877	3.0	Gain	0
Chr21	9,825,948	32,965,213	3.0	Gain	265
Chr21	35,230,780	38,009,239	3.0	Gain	60
Chr21	44,783,270	44,838,097	3.0	Gain	17
Chr21	44,841,036	46,020,721	4.0	Gain	97
Chr21	46,021,088	46,419,158	3.0	Gain	37
Chr21	47,546,244	47,614,660	3.0	Gain	13
Chr21	47,616,071	48,078,611	4.0	Gain	0

CNVs in chromosome 11 constituted >20% of all CNVs in the MFH+P sample.
Abbreviations: Chr, chromosome; CNV, copy number variation; SNP, single nucleotide polymorphism.

[Fig. 4(e)] revealed the remarkable overexpression of CYP24A1, which is a target gene of the VDR and inactivates 1,25-dihydroxyvitamin D3 via 24-hydroxylation. Our microarray panel showed that among the five MFHs examined, CYP24A1 was expressed at the greatest level in our MFH+P compared with the four other non–PTH-producing MFHs [Fig. 4(e)]. Our qRT-PCR assay confirmed that the MFH GSM149194 expressed CYP24A1 mRNA at less than 1/100th of the level observed in MFH+P cells. The two PAs did not express CYP24A1 [Fig. 4(e)]. These results suggest that CYP24A1 itself might be deeply involved in ectopic PTH production in MFH+P cells [7–14]. In contrast, CYP24A1 mRNA levels varied in various cultured cancer cells [Fig. 4(e)].

The CYP24A1 gene is potently suppressed by the HIC1 tumor suppressor [15–17]. Microarray profiling revealed that the four non–PTH-producing MFHs expressed sixfold or greater levels of HIC1 mRNA than the MFH+P [Fig. 4(a)], and a subsequent qRT-PCR assay revealed that the MFH+P expressed <30-fold HIC1 mRNA compared with MFH GSM149194 (data not shown). Although unconfirmed, these data suggest that HIC1 underexpression might trigger CYP24A1 overexpression in MFH+P cells [15–17].

G. Immunofluorescence Microscopy

Next, the expression of CYP24A1, VDR, and CaSR was compared between PA and MFH+P cells by immunofluorescence microscopy [Fig. 5(a–c)]. We found that all the data obtained at the protein level were concordant with the corresponding qRT-PCR data at the mRNA level. CYP24A1 protein was highly expressed in MFH+P cells but not in PA cells. In contrast, CaSR protein was exclusively present on the surface of PA cells but not MFH+P cells. Finally, the level of VDR was quite different between the two, with greater amounts of VDR observed in the PA sample. This finding might also explain the notable lack of the vitamin D–VDR signaling system in the MFH+P. These data, along with the mRNA content of each cell type, are summarized in Fig. 5(d).

H. lncRNA Recognized Only in the PA and PTH-Producing MFH+P Samples

Finally, we explored whether lncRNAs are another candidate driver of the commonality in PTH overexpression. The DNA sequences in the 3′-flanking region of the human PTH gene are responsible for calcium- and phosphate-mediated PTH gene regulation, although the exact location or specific players interacting with the DNA/RNA sequences remain partially unknown [70, 71]. After a random serial qRT-PCR survey using primers scattered 20 to 50 kbp downstream of the human PTH gene to identify tissue-specific transcripts, we detected several distinct species of lncRNA of 800 to 3800 bases in length (data not shown). The expression of at least one of these lncRNAs of 2533 bases covering no PTH exonic sequence

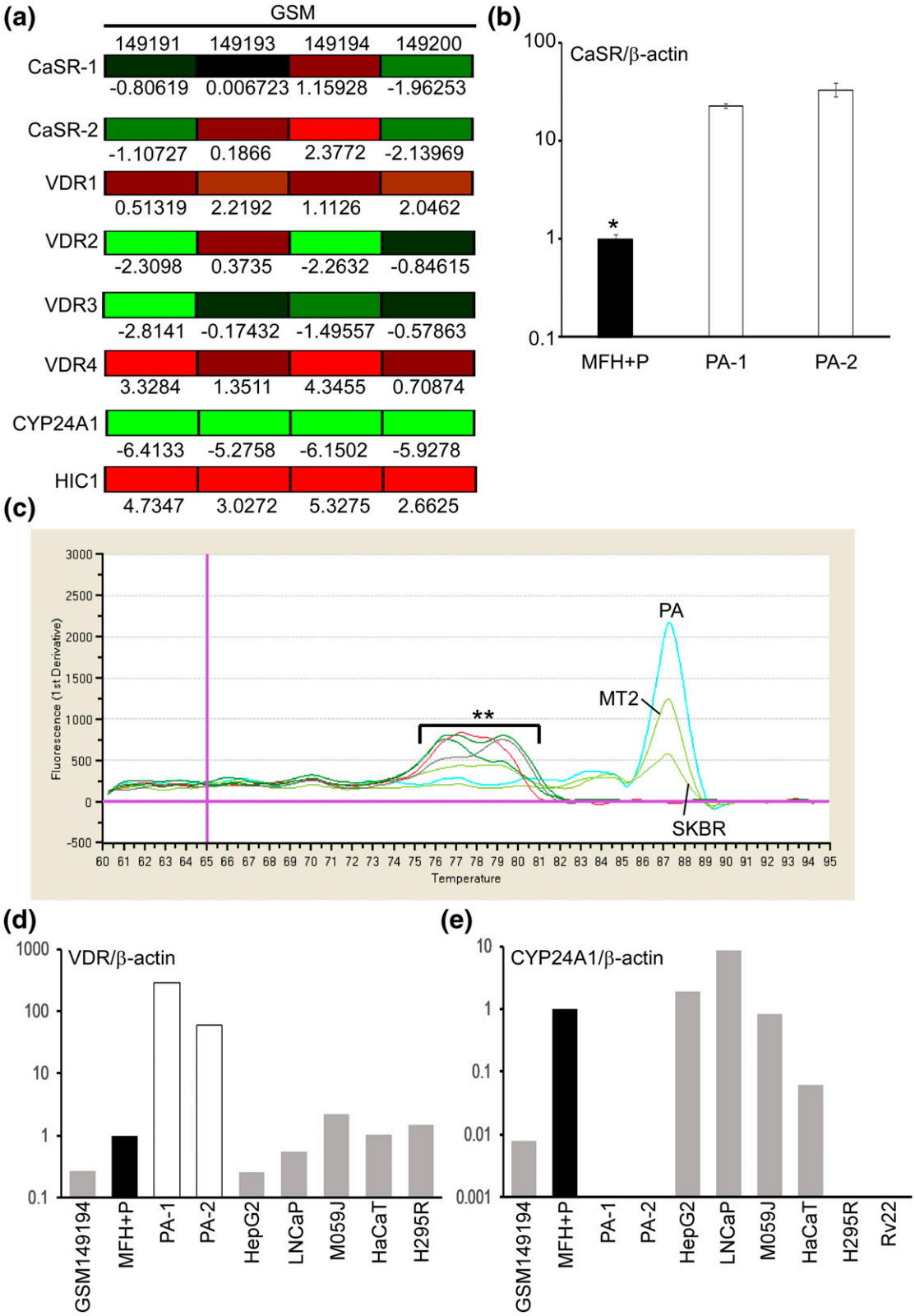

Figure 4. CaSR mRNA by microarray and real-time qRT-PCR. (a) Comparison among the MFH+P and the four other MFHs. Data were obtained from the registered microarray panel [45]. (Left) The corresponding heatmap is indicated. Green-to-red corresponds to elevated-to-reduced expression compared with that in the MFH+P. Two (CaSR) and four (VDR) different

probe sets were used. For CYP24A1 and HIC1 mRNAs, only one probe was used, respectively. Numbers with a minus sign indicate an increase, and those without indicate a decrease in the mRNA level in MFH+P cells compared with each MFH (represented as an exponent of 2). (b) qRT-PCR of CaSR/β-actin mRNA. MFH+P (black) and two different preparations of PAs (white). The MFH+P number (approximately 1, which was tagged with an asterisk) was probably of no significance (see Fig. c). (c) Dissociation curves of the amplified cDNAs other than those derived from PA, MT2, and SKBR cells suggested that these nonparathyroid cells do not express substantial levels of CaSR mRNA. **MFH+P, HepG2 (hepatoma), M059J (glioma), HaCaT (keratinocyte), H295R (adrenocortical), and RV22 (prostate cancer) cells. (d) qRT-PCR of VDR/β-actin in MFH-P (GSM149194), MFH+P (black), two PAs, and other cultured cells. *LNCaP cells represent LNCaP cells treated with 1,25-dihydroxyvitamin D3 (10^{-8} M) for 24 hours. (e) qRT-PCR of CYP24A1/β-actin in MFH-P (GSM149194), MFH+P (black), two PAs (white), and other cultured cells. Two separate preparations of PAs yielded no PCR products. To validate the qRT-PCR data with (c) CaSR, (d) VDR, and (e) CYP24A1, we used two different sets of primers covering separate positions of each cDNA. In each, the data were similar and the results from one set are shown.

(Fig. 6, region A) was exclusively found in the PA and MFH+P samples but not in the other cultured cancer cell lines examined. GAPDH mRNA expression was analyzed among the samples using qRT-PCR, and it varied less than threefold in all samples (data not shown). Our observation that other sets of RT-PCR primers adjacent to this 2533-base region did not capture any nucleic acids in these cells confirmed that our samples, except for the positive control, did not contain detectable amounts of residual DNA. Furthermore, the nucleotide sequence of this lncRNA did not match any other in open or public databases of lncRNA, such as LNCipedia (available at: http://www.lncipedia.org/) or NONCODE (available at: http://www.noncode.org/), suggesting this is an lncRNA expressed within a very narrow range of cell types.

3. Discussion

Our study included only one ectopic PTH-producing tumor. Notwithstanding, to the best of our knowledge, our report of this extremely rare tumor uses microarray data mining and whole exome sequencing. We believe that our findings could be a scaffold for understanding the pathogenesis of ectopic PTH-producing tumors.

We found that the levels of various transcription factors determining parathyroid differentiation during development, including transcription factors involved in PTH gene expression [48, 53–63], were not significantly dysregulated in the MFH+P (Figs. 2 and 3).

Whole exome sequencing revealed a frameshift mutation in the ATRX gene [64] (Table 3). Defects in ATRX have been shown to be a driver for pancreatic neuroendocrine tumors; however, these mutations have never been linked to PTH expression [64–66]. In addition, the significance of the copy number variation observed in chromosome 11 in the MFH+P (Table 4) remains unknown.

We explored the behavior of CaSR in our samples. CaSR expression was almost undetectable in the MFH+P [Figs. 4(a–c) and 5(c)], suggesting a close relationship between the absence of CaSR and PTH expression. Lethal hypercalcemia in mice and humans can be induced by systemic inactivity of the CaSR gene and PTH overexpression in the parathyroid [39–41]. Thus, if any first hit triggers PTH production in nonparathyroid cells, a chance might exist that its expression would be reinforced via disruption of the CaSR signal transduction system [72–75]. The absence of CaSR in the adult parathyroid has been reported to be a possible trigger for parathyroid tumor formation [76].

Our microarray profiling revealed robust CYP24A1 mRNA expression in the MFH+P [Fig. 4(e)] compared with the other MFH GSM149194. Ablation of the vitamin D–VDR signaling system by whole-body VDR disruption increases PTH expression in the parathyroid gland but not in nonparathyroid cells elsewhere [56, 73, 77–81]. Our qRT-PCR and immunofluorescence analyses showed that CYP24A1 was barely present in the PA [Figs. 4(e) and 5(a)]. Therefore,

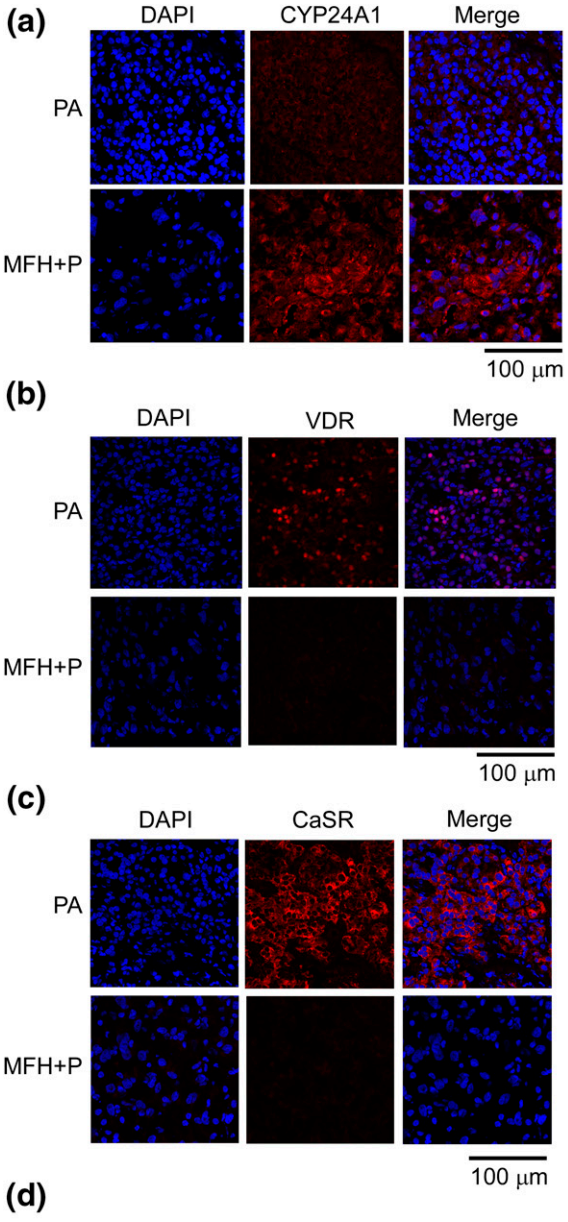

(d)

	CaSR protein	CYP24A1 protein	HIC1 mRNA	VDR protein	PTH protein
Parathyroid adenoma	↑↑↑↑	0	0	↑↑↑↑	↑↑↑↑↑
Normal parathyroid (48,66)	↑↑↑↑↑	?	?	↑↑↑↑↑	↑↑↑↑
MFH+P	0	↑↑↑↑↑	↑	↑↑	↑↑↑↑
MFH-P (GSM149194)	0	↑	↑↑↑↑↑	↑	0

Figure 5. Expression of (a) CaSR, (b) VDR, and (c) CYP24A1 examined by immunostaining. (d) A summary is also provided. (d) The data regarding the normal parathyroid were obtained from Sudhaker Rao *et al.* [69] and Corbett *et al.* [87], which compared the amounts of the indicated items between parathyroid adenoma and normal parathyroid. In each figure, the MFH+P cells (top three panels) and PA cells (bottom three panels) were fixed with 4% paraformaldehyde and stained with each antibody. Red staining indicates data obtained using each antibody, and blue staining shows 496-diamidine-29-phenylindole dihydrochloride (DAPI) (cell nuclei). Scale bars = 100 μm.

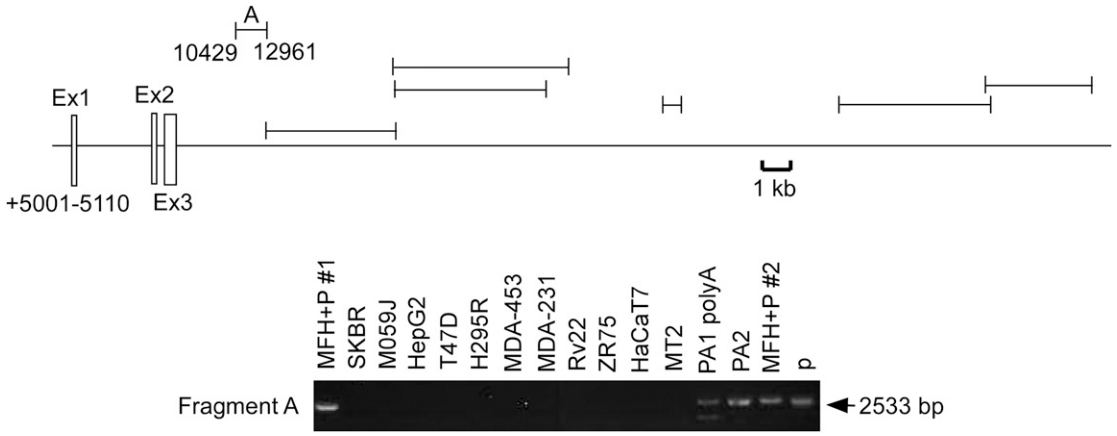

Figure 6. lncRNA. After random scanning with real-time qRT-PCR using various primers to search for tissue-specific transcripts, the 2- to 5-kbp candidate region spanning each primer set that yielded positive results in this screening was amplified for lncRNA detection, and the samples were loaded onto a 0.9% agarose gel. "P" denotes a positive control obtained from a crude mRNA fraction of MCF-7 cells in which certain amounts of residual genomic DNA were left after no further DNase treatment. GAPDH mRNA expression in the samples was analyzed by qRT-PCR, and the differences among them were all less than threefold (data not shown). The position of the start point of exon 1 was arbitrarily marked as 5001. Transcripts from the region denoted as "A" were detected. The six other 3′-flanking positions shown were not amplified even in the PA and MFH+P samples. In contrast, the positive control containing genomic DNA was clearly amplified in each case (data not shown). These results also support the validity of the lncRNA in our RNA samples from the PA and MFH+P tumors. "MFH+P-2" denotes the cDNA from the same MFH+P obtained on a different occasion.

once PTH expression occurs by unknown mechanisms, intratumor hypovitaminosis D might be related to the tumorigenesis of MFH+P. CYP24A1 overexpression as an oncogene or an intracellular repressor of active vitamin D signaling might play a provocative role in the development of several cancers [28–35]. HIC1 is a tumor suppressor gene [36]. We found the MFH+P-specific underexpression of HIC1 mRNA [Fig. 4(a)]. Because HIC1 also represses CYP24A1 expression [37, 38, 82], these data suggest that HIC1 underexpression might trigger CYP24A1 overexpression in MFH+P.

These three combinations (PTH overproduction, lack of CaSR expression, overexpression of CYP24A1, and the paucity of the two braking systems) are summarized in Fig. 5(d). However, the combination of a large amount of CYP24A1 protein in the absence of CaSR is not a rare event [Fig. 4(a–c) and 4(e)], implying that both molecules cannot be *bona fide* MFH+P drivers, However, our discovery that an lncRNA in a nonexonic region of the human PTH gene is expressed exclusively in the PA and MFH+P (Fig. 6) raises the possibility that this lncRNA might be one of the long sought-after factors determining PTH expression, although this hypothesis is totally speculative at present. Recent work has identified lncRNAs as tumorigenesis promoters, chromatin modifiers, and, especially, tissue-specific expression regulators [41–43, 83]. Because transfectable PTH-producing cells are unavailable, the exogenous overexpression of this RNA in either direction in various non–PTH-producing cultured cells would clarify its role in PTH production.

PTHrP stimulates CYP27B1 *in vitro* via PT1R, identical to the PTH receptor. However, serum $1,25(OH)_2$ vitamin D3 levels in humoral hypercalcemia of malignancy due to PTHrP overexpression are often low, just as was seen in our MFH+P (Table 2). Although speculative, some inhibitory molecules for CYP27B1 production postulated in such cases [84–86] might also be involved in our MFH+P, which could be an accelerator of CYP24D1 in turn.

Overall, the similarities and dissimilarities of the PTH-regulator molecules among the PA, PTH-producing MFH, and non–PTH-producing MFH samples would provide us with a dynamic profile of potential pathogenic factors.

Acknowledgments

Current affiliation: Y. Ikeda's current affiliation is the Department of Surgery, International University of Health and Welfare, Mita Hospital, Tokyo 108-8329, Japan.

Address all correspondence to: Masayoshi Iizuka, MD, PhD, Department of Biochemistry, Teikyo University School of Medicine, 2-11-1 Kaga, Itabashi-ku, Tokyo 173-8605, Japan. E-mail: miizuka@med.teikyo-u.ac.jp.

M.I., M.T.-A., T.S., and T.O. were supported by the Japan Society for the Promotion of Science Grants-in-Aid for Scientific Research (Grants JP26460400, JP15K08286, JP16K20163, and JP24591372).

Author contributions: K.U., M.T.-A., K.M., T.O., and Y.T. designed the study; K.U., M.I., H.I., K.M., H.F., G.N., Y.I., H.A., and T.O. processed the samples and supervised the microarray analyses and exome sequencing; K.U., M.I., T.S., H.F., M.T.-A., and T.O. performed the computational and graphical analyses; K.U., M.W., H.I., K.M., H.F., M.I., G.Y., M.T.-A., and Y.T. coordinated sample acquisition; M.W., M.T.-A., T.F., and H.U. performed the pathological review and analysis; K.U., M.I., S.M., H.F., T.S., M.T.-A., and T.O. performed the *in vitro* experiments; H.O. supported the maintenance of the experiments; K.U., M.I., M.T.-A., and T.O. wrote the manuscript; and M.I., G.Y., H.O., and Y.T. were involved in critical review and discussion.

Disclosure Summary: The authors have nothing to disclose.

References and Notes

1. Martin TJ. Parathyroid hormone-related protein, its regulation of cartilage and bone development, and role in treating bone diseases. *Physiol Rev*. 2016;**96**(3):831–871.
2. Mundy GR, Edwards JR. PTH-related peptide (PTHrP) in hypercalcemia. *J Am Soc Nephrol*. 2008; **19**(4):672–675.
3. Mayer S, Cypess AM, Kocher ON, Berman SM, Huberman MS, Hartzband PI, Halmos B. Uncommon presentations of some common malignancies: case 1. Sequential paraneoplastic endocrine syndromes in small-cell lung cancer. *J Clin Oncol*. 2005;**23**(6):1312–1314.
4. Nussbaum SR, Gaz RD, Arnold A. Hypercalcemia and ectopic secretion of parathyroid hormone by an ovarian carcinoma with rearrangement of the gene for parathyroid hormone. *N Engl J Med*. 1990; **323**(19):1324–1328.
5. VanHouten JN, Yu N, Rimm D, Dotto J, Arnold A, Wysolmerski JJ, Udelsman R. Hypercalcemia of malignancy due to ectopic transactivation of the parathyroid hormone gene. *J Clin Endocrinol Metab*. 2006;**91**(2):580–583.
6. Yoshimoto K, Yamasaki R, Sakai H, Tezuka U, Takahashi M, Iizuka M, Sekiya T, Saito S. Ectopic production of parathyroid hormone by small cell lung cancer in a patient with hypercalcemia. *J Clin Endocrinol Metab*. 1989;**68**(5):976–981.
7. Buller R, Taylor K, Burg AC, Berman ML, DiSaia PJ. Paraneoplastic hypercalcemia associated with adenosquamous carcinoma of the endometrium. *Gynecol Oncol*. 1991;**40**(1):95–98.
8. Strewler GJ, Budayr AA, Clark OH, Nissenson RA. Production of parathyroid hormone by a malignant nonparathyroid tumor in a hypercalcemic patient. *J Clin Endocrinol Metab*. 1993;**76**(5): 1373–1375.
9. Rizzoli R, Pache JC, Didierjean L, Bürger A, Bonjour JP. A thymoma as a cause of true ectopic hyperparathyroidism. *J Clin Endocrinol Metab*. 1994;**79**(3):912–915.
10. Nielsen PK, Rasmussen AK, Feldt-Rasmussen U, Brandt M, Christensen L, Olgaard K. Ectopic production of intact parathyroid hormone by a squamous cell lung carcinoma in vivo and in vitro. *J Clin Endocrinol Metab*. 1996;**81**(10):3793–3796.
11. Iguchi H, Miyagi C, Tomita K, Kawauchi S, Nozuka Y, Tsuneyoshi M, Wakasugi H. Hypercalcemia caused by ectopic production of parathyroid hormone in a patient with papillary adenocarcinoma of the thyroid gland. *J Clin Endocrinol Metab*. 1998;**83**(8):2653–2657.
12. Koyama Y, Ishijima H, Ishibashi A, Katsuya T, Ishizaka H, Aoki J, Endo K. Intact PTH-producing hepatocellular carcinoma treated by transcatheter arterial embolization. *Abdom Imaging*. 1999;**24**(2): 144–146.
13. Uchimura K, Mokuno T, Nagasaka A, Hayakawa N, Kato T, Yamazaki N, Kobayashi T, Nagata M, Kotake M, Itoh M, Tsujimura T, Iwase K. Lung cancer associated with hypercalcemia induced by concurrently elevated parathyroid hormone and parathyroid hormone-related protein levels. *Metabolism*. 2002;**51**(7):871–875.

14. Botea V, Edelson GW, Munasinghe RL. Hyperparathyroidism, hypercalcemia, and calcified brain metastatic lesions in a patient with small cell carcinoma demonstrating positive immunostain for parathyroid hormone. *Endocr Pract*. 2003;**9**(1):40–44.
15. Ohira S, Itoh K, Shiozawa T, Horiuchi A, Ono K, Takeuchi H, Hosoda W, Konishi I. Ovarian non-small cell neuroendocrine carcinoma with paraneoplastic parathyroid hormone-related hypercalcemia. *Int J Gynecol Pathol*. 2004;**23**(4):393–397.
16. Chen L, Dinh TA, Haque A. Small cell carcinoma of the ovary with hypercalcemia and ectopic parathyroid hormone production. *Arch Pathol Lab Med*. 2005;**129**(4):531–533.
17. Wong K, Tsuda S, Mukai R, Sumida K, Arakaki R. Parathyroid hormone expression in a patient with metastatic nasopharyngeal rhabdomyosarcoma and hypercalcemia. *Endocrine*. 2005;**27**(1):83–86.
18. Vacher-Coponat H, Opris A, Denizot A, Dussol B, Berland Y. Hypercalcaemia induced by excessive parathyroid hormone secretion in a patient with a neuroendocrine tumour. *Nephrol Dial Transplant*. 2005;**20**(12):2832–2835.
19. Bhattacharya A, Mittal BR, Bhansali A, Radotra BD, Behera A. Cervical paraganglioma mimicking a parathyroid adenoma on Tc-99m sestamibi scintigraphy. *Clin Nucl Med*. 2006;**31**(4):234–236.
20. Mahoney EJ, Monchik JM, Donatini G, De Lellis R. Life-threatening hypercalcemia from a hepatocellular carcinoma secreting intact parathyroid hormone: localization by sestamibi single-photon emission computed tomographic imaging. *Endocr Pract*. 2006;**12**(3):302–306.
21. Morita SY, Brownlee NA, Dackiw AP, Westra WH, Clark DP, Zeiger MA. An unusual case of recurrent hyperparathyroidism and papillary thyroid cancer. *Endocr Pract*. 2009;**15**(4):349–352.
22. Demura M, Yoneda T, Wang F, Zen Y, Karashima S, Zhu A, Cheng Y, Yamagishi M, Takeda Y. Ectopic production of parathyroid hormone in a patient with sporadic medullary thyroid cancer. *Endocr J*. 2010; **57**(2):161–170.
23. Kandil E, Noureldine S, Khalek MA, Daroca P, Friedlander P. Ectopic secretion of parathyroid hormone in a neuroendocrine tumor: a case report and review of the literature. *Int J Clin Exp Med*. 2011;**4**(3): 234–240.
24. Bernini M, Bacca A, Casto G, Carli V, Cupisti A, Carrara D, Farnesi I, Barsotti G, Naccarato AG, Bernini G. A case of pheochromocytoma presenting as secondary hyperaldosteronism, hyperparathyroidism, diabetes and proteinuric renal disease. *Nephrol Dial Transplant*. 2011;**26**(3):1104–1107.
25. Abe Y, Makiyama H, Fujita Y, Tachibana Y, Kamada G, Uebayashi M. Severe hypercalcemia associated with hepatocellular carcinoma secreting intact parathyroid hormone: a case report. *Intern Med*. 2011; **50**(4):329–333.
26. Nakajima K, Tamai M, Okaniwa S, Nakamura Y, Kobayashi M, Niwa T, Horigome N, Ito N, Suzuki S, Nishio S, Komatsu M. Humoral hypercalcemia associated with gastric carcinoma secreting parathyroid hormone: a case report and review of the literature. *Endocr J*. 2013;**60**(5):557–562.
27. St-Arnaud R, Arabian A, Travers R, Barletta F, Raval-Pandya M, Chapin K, Depovere J, Mathieu C, Christakos S, Demay MB, Glorieux FH. Deficient mineralization of intramembranous bone in vitamin D-24-hydroxylase-ablated mice is due to elevated 1,25-dihydroxyvitamin D and not to the absence of 24,25-dihydroxyvitamin D. *Endocrinology*. 2000;**141**(7):2658–2666.
28. Albertson DG, Ylstra B, Segraves R, Collins C, Dairkee SH, Kowbel D, Kuo WL, Gray JW, Pinkel D. Quantitative mapping of amplicon structure by array CGH identifies CYP24 as a candidate oncogene. *Nat Genet*. 2000;**25**(2):144–146.
29. Luo W, Hershberger PA, Trump DL, Johnson CS. 24-Hydroxylase in cancer: impact on vitamin D-based anticancer therapeutics. *J Steroid Biochem Mol Biol*. 2013;**136**:252–257.
30. So JY, Suh N. Targeting cancer stem cells in solid tumors by vitamin D. *J Steroid Biochem Mol Biol*. 2015;**148**:79–85.
31. Parise RA, Egorin MJ, Kanterewicz B, Taimi M, Petkovich M, Lew AM, Chuang SS, Nichols M, El-Hefnawy T, Hershberger PA. CYP24, the enzyme that catabolizes the antiproliferative agent vitamin D, is increased in lung cancer. *Int J Cancer*. 2006;**119**(8):1819–1828.
32. Cross HS, Nittke T, Kallay E. Colonic vitamin D metabolism: implications for the pathogenesis of inflammatory bowel disease and colorectal cancer. *Mol Cell Endocrinol*. 2011;**347**(1-2):70–79.
33. Horváth HC, Lakatos P, Kósa JP, Bácsi K, Borka K, Bises G, Nittke T, Hershberger PA, Speer G, Kállay E. The candidate oncogene CYP24A1: a potential biomarker for colorectal tumorigenesis. *J Histochem Cytochem*. 2010;**58**(3):277–285.
34. King AN, Beer DG, Christensen PJ, Simpson RU, Ramnath N. The vitamin D/CYP24A1 story in cancer. *Anticancer Agents Med Chem*. 2010;**10**(3):213–224.
35. Zhalehjoo N, Shakiba Y, Panjehpour M. Gene expression profiles of CYP24A1 and CYP27B1 in malignant and normal breast tissues. *Mol Med Rep*. 2017;**15**(1):467–473.

36. Svedlund J, Koskinen Edblom S, Marquez VE, Åkerström G, Björklund P, Westin G. Hypermethylated in cancer 1 (HIC1), a tumor suppressor gene epigenetically deregulated in hyperparathyroid tumors by histone H3 lysine modification. *J Clin Endocrinol Metab*. 2012;**97**(7):E1307–E1315.
37. Borkowski R, Du L, Zhao Z, McMillan E, Kosti A, Yang CR, Suraokar M, Wistuba II, Gazdar AF, Minna JD, White MA, Pertsemlidis A. Genetic mutation of p53 and suppression of the miR-17~92 cluster are synthetic lethal in non-small cell lung cancer due to upregulation of vitamin D signaling. *Cancer Res*. 2015;**75**(4):666–675.
38. Van Rechem C, Rood BR, Touka M, Pinte S, Jenal M, Guérardel C, Ramsey K, Monté D, Bégue A, Tschan MP, Stephan DA, Leprince D. Scavenger chemokine (CXC motif) receptor 7 (CXCR7) is a direct target gene of HIC1 (hypermethylated in cancer 1). *J Biol Chem*. 2009;**284**(31):20927–20935.
39. Pollak MR, Brown EM, Chou YH, Hebert SC, Marx SJ, Steinmann B, Levi T, Seidman CE, Seidman JG. Mutations in the human Ca(2+)-sensing receptor gene cause familial hypocalciuric hypercalcemia and neonatal severe hyperparathyroidism. *Cell*. 1993;**75**(7):1297–1303.
40. Brown EM. Familial hypocalciuric hypercalcemia and other disorders with resistance to extracellular calcium. *Endocrinol Metab Clin North Am*. 2000;**29**(3):503–522.
41. Hendy GN, D'Souza-Li L, Yang B, Canaff L, Cole DE. Mutations of the calcium-sensing receptor (CASR) in familial hypocalciuric hypercalcemia, neonatal severe hyperparathyroidism, and autosomal dominant hypocalcemia. *Hum Mutat*. 2000;**16**(4):281–296.
42. Huarte M. The emerging role of lncRNAs in cancer. *Nat Med*. 2015;**21**(11):1253–1261.
43. Knoll M, Lodish HF, Sun L. Long non-coding RNAs as regulators of the endocrine system. *Nat Rev Endocrinol*. 2015;**11**(3):151–160.
44. Fatica A, Bozzoni I. Long non-coding RNAs: new players in cell differentiation and development. *Nat Rev Genet*. 2014;**15**(1):7–21.
45. Nakayama R, Nemoto T, Takahashi H, Ohta T, Kawai A, Seki K, Yoshida T, Toyama Y, Ichikawa H, Hasegawa T. Gene expression analysis of soft tissue sarcomas: characterization and reclassification of malignant fibrous histiocytoma. *Mod Pathol*. 2007;**20**(7):749–759.
46. Fujii H, Tamamori-Adachi M, Uchida K, Susa T, Nakakura T, Hagiwara H, Iizuka M, Okinaga H, Tanaka Y, Okazaki T. Marked cortisol production by intracrine ACTH in GIP-treated cultured adrenal cells in which the GIP receptor was exogenously introduced. *PLoS One*. 2014;**9**(10):e110543.
47. Kakiuchi M, Nishizawa T, Ueda H, Gotoh K, Tanaka A, Hayashi A, Yamamoto S, Tatsuno K, Katoh H, Watanabe Y, Ichimura T, Ushiku T, Funahashi S, Tateishi K, Wada I, Shimizu N, Nomura S, Koike K, Seto Y, Fukayama M, Aburatani H, Ishikawa S. Recurrent gain-of-function mutations of RHOA in diffuse-type gastric carcinoma. *Nat Genet*. 2014;**46**(6):583–587.
48. Alimov AP, Park-Sarge OK, Sarge KD, Malluche HH, Koszewski NJ. Transactivation of the parathyroid hormone promoter by specificity proteins and the nuclear factor Y complex. *Endocrinology*. 2005;**146**(8):3409–3416.
49. Costa-Guda J, Soong CP, Parekh VI, Agarwal SK, Arnold A. Germline and somatic mutations in cyclin-dependent kinase inhibitor genes CDKN1A, CDKN2B, and CDKN2C in sporadic parathyroid adenomas. *Horm Cancer*. 2013;**4**(5):301–307.
50. Imanishi Y, Hosokawa Y, Yoshimoto K, Schipani E, Mallya S, Papanikolaou A, Kifor O, Tokura T, Sablosky M, Ledgard F, Gronowicz G, Wang TC, Schmidt EV, Hall C, Brown EM, Bronson R, Arnold A. Primary hyperparathyroidism caused by parathyroid-targeted overexpression of cyclin D1 in transgenic mice. *J Clin Invest*. 2001;**107**(9):1093–1102.
51. Mallya SM, Wu HI, Saria EA, Corrado KR, Arnold A. Tissue-specific regulatory regions of the PTH gene localized by novel chromosome 11 rearrangement breakpoints in a parathyroid adenoma. *J Bone Miner Res*. 2010;**25**(12):2606–2612.
52. Olauson H, Lindberg K, Amin R, Sato T, Jia T, Goetz R, Mohammadi M, Andersson G, Lanske B, Larsson TE. Parathyroid-specific deletion of Klotho unravels a novel calcineurin-dependent FGF23 signaling pathway that regulates PTH secretion. *PLoS Genet*. 2013;**9**(12):e1003975.
53. Grigorieva IV, Thakker RV. Transcription factors in parathyroid development: lessons from hypoparathyroid disorders. *Ann N Y Acad Sci*. 2011;**1237**:24–38.
54. Sulaiman L, Nilsson IL, Juhlin CC, Haglund F, Höög A, Larsson C, Hashemi J. Genetic characterization of large parathyroid adenomas. *Endocr Relat Cancer*. 2012;**19**(3):389–407.
55. Westin G. Molecular genetics and epigenetics of nonfamilial (sporadic) parathyroid tumours. *J Intern Med*. 2016;**280**(6):551–558.
56. Günther T, Chen ZF, Kim J, Priemel M, Rueger JM, Amling M, Moseley JM, Martin TJ, Anderson DJ, Karsenty G. Genetic ablation of parathyroid glands reveals another source of parathyroid hormone. *Nature*. 2000;**406**(6792):199–203.

57. Li Q, Herrler M, Landsberger N, Kaludov N, Ogryzko VV, Nakatani Y, Wolffe AP. Xenopus NF-Y presets chromatin to potentiate p300 and acetylation-responsive transcription from the Xenopus hsp70 promoter in vivo. *EMBO J*. 1998;**17**(21):6300–6315.
58. Huang W, Zhao S, Ammanamanchi S, Brattain M, Venkatasubbarao K, Freeman JW. Trichostatin A induces transforming growth factor beta type II receptor promoter activity and acetylation of Sp1 by recruitment of PCAF/p300 to a Sp1.NF-Y complex. *J Biol Chem*. 2005;**280**(11):10047–10054.
59. Hughes R, Kristiansen M, Lassot I, Desagher S, Mantovani R, Ham J. NF-Y is essential for expression of the proapoptotic bim gene in sympathetic neurons. *Cell Death Differ*. 2011;**18**(6):937–947.
60. Nechama M, Uchida T, Mor Yosef-Levi I, Silver J, Naveh-Many T. The peptidyl-prolyl isomerase Pin1 determines parathyroid hormone mRNA levels and stability in rat models of secondary hyperparathyroidism. *J Clin Invest*. 2009;**119**(10):3102–3114.
61. Okazaki T, Ando K, Igarashi T, Ogata E, Fujita T. Conserved mechanism of negative gene regulation by extracellular calcium: parathyroid hormone gene versus atrial natriuretic polypeptide gene. *J Clin Invest*. 1992;**89**(4):1268–1273.
62. Okazaki T, Chung U, Nishishita T, Ebisu S, Usuda S, Mishiro S, Xanthoudakis S, Igarashi T, Ogata E. A redox factor protein, ref1, is involved in negative gene regulation by extracellular calcium. *J Biol Chem*. 1994;**269**(45):27855–27862.
63. Chung U, Igarashi T, Nishishita T, Iwanari H, Iwamatsu A, Suwa A, Mimori T, Hata K, Ebisu S, Ogata E, Fujita T, Okazaki T. The interaction between Ku antigen and REF1 protein mediates negative gene regulation by extracellular calcium. *J Biol Chem*. 1996;**271**(15):8593–8598.
64. Jiao Y, Shi C, Edil BH, de Wilde RF, Klimstra DS, Maitra A, Schulick RD, Tang LH, Wolfgang CL, Choti MA, Velculescu VE, Diaz LA Jr, Vogelstein B, Kinzler KW, Hruban RH, Papadopoulos N. DAXX/ATRX, MEN1, and mTOR pathway genes are frequently altered in pancreatic neuroendocrine tumors. *Science*. 2011;**331**(6021):1199–1203.
65. Heaphy CM, de Wilde RF, Jiao Y, Klein AP, Edil BH, Shi C, Bettegowda C, Rodriguez FJ, Eberhart CG, Hebbar S, Offerhaus GJ, McLendon R, Rasheed BA, He Y, Yan H, Bigner DD, Oba-Shinjo SM, Marie SK, Riggins GJ, Kinzler KW, Vogelstein B, Hruban RH, Maitra A, Papadopoulos N, Meeker AK. Altered telomeres in tumors with ATRX and DAXX mutations. *Science*. 2011;**333**(6041):425.
66. Wong LH, McGhie JD, Sim M, Anderson MA, Ahn S, Hannan RD, George AJ, Morgan KA, Mann JR, Choo KH. ATRX interacts with H3.3 in maintaining telomere structural integrity in pluripotent embryonic stem cells. *Genome Res*. 2010;**20**(3):351–360.
67. Cromer MK, Starker LF, Choi M, Udelsman R, Nelson-Williams C, Lifton RP, Carling T. Identification of somatic mutations in parathyroid tumors using whole-exome sequencing. *J Clin Endocrinol Metab*. 2012;**97**(9):E1774–E1781.
68. Yi Y, Nowak NJ, Pacchia AL, Morrison C. Chromosome 11 genomic changes in parathyroid adenoma and hyperplasia: array CGH, FISH, and tissue microarrays. *Genes Chromosomes Cancer*. 2008;**47**(8):639–648.
69. Sudhaker Rao D, Han ZH, Phillips ER, Palnitkar S, Parfitt AM. Reduced vitamin D receptor expression in parathyroid adenomas: implications for pathogenesis. *Clin Endocrinol (Oxf)*. 2000;**53**(3):373–381.
70. Naveh-Many T. Minireview: the play of proteins on the parathyroid hormone messenger ribonucleic acid regulates its expression. *Endocrinology*. 2010;**151**(4):1398–1402.
71. Lavi-Moshayoff V, Silver J, Naveh-Many T. Human PTH gene regulation in vivo using transgenic mice. *Am J Physiol Renal Physiol*. 2009;**297**(3):F713–F719.
72. Brennan SC, Thiem U, Roth S, Aggarwal A, Fetahu IS, Tennakoon S, Gomes AR, Brandi ML, Bruggeman F, Mentaverri R, Riccardi D, Kallay E. Calcium sensing receptor signalling in physiology and cancer. *Biochim Biophys Acta*. 2013;**1833**(7):1732–1744.
73. Bikle DD, Jiang Y, Nguyen T, Oda Y, Tu CL. Disruption of vitamin D and calcium signaling in keratinocytes predisposes to skin cancer. *Front Physiol*. 2016;**7**:296.
74. Tae CH, Shim KN, Kim HI, Joo YH, Lee JH, Cho MS, Moon CM, Kim SE, Jung HK, Jung SA. Significance of calcium-sensing receptor expression in gastric cancer. *Scand J Gastroenterol*. 2016;**51**(1):67–72.
75. Aggarwal A, Kállay E. Cross talk between the calcium-sensing receptor and the vitamin D system in prevention of cancer. *Front Physiol*. 2016;**7**:451.
76. Burski K, Torjussen B, Paulsen AQ, Boman H, Bollerslev J. Parathyroid adenoma in a subject with familial hypocalciuric hypercalcemia: coincidence or causality? *J Clin Endocrinol Metab*. 2002;**87**(3):1015–1016.
77. Velázquez-Fernández D, Laurell C, Saqui-Salces M, Pantoja JP, Candanedo-Gonzalez F, Reza-Albarrán A, Gamboa-Dominguez A, Herrera MF. Differential RNA expression profile by cDNA

microarray in sporadic primary hyperparathyroidism (pHPT): primary parathyroid hyperplasia versus adenoma. *World J Surg*. 2006;**30**(5):705–713.

78. Meir T, Levi R, Lieben L, Libutti S, Carmeliet G, Bouillon R, Silver J, Naveh-Many T. Deletion of the vitamin D receptor specifically in the parathyroid demonstrates a limited role for the receptor in parathyroid physiology. *Am J Physiol Renal Physiol*. 2009;**297**(5):F1192–F1198.
79. Yoshizawa T, Handa Y, Uematsu Y, Takeda S, Sekine K, Yoshihara Y, Kawakami T, Arioka K, Sato H, Uchiyama Y, Masushige S, Fukamizu A, Matsumoto T, Kato S. Mice lacking the vitamin D receptor exhibit impaired bone formation, uterine hypoplasia and growth retardation after weaning. *Nat Genet*. 1997;**16**(4):391–396.
80. Sakai Y, Kishimoto J, Demay MB. Metabolic and cellular analysis of alopecia in vitamin D receptor knockout mice. *J Clin Invest*. 2001;**107**(8):961–966.
81. Silverberg SJ. Vitamin D deficiency and primary hyperparathyroidism. *J Bone Miner Res*. 2007;**22** (Suppl 2):V100–V104.
82. Fleuriel C, Touka M, Boulay G, Guérardel C, Rood BR, Leprince D. HIC1 (hypermethylated in cancer 1) epigenetic silencing in tumors. *Int J Biochem Cell Biol*. 2009;**41**(1):26–33.
83. Clark MB, Mercer TR, Bussotti G, Leonardi T, Haynes KR, Crawford J, Brunck ME, Cao KA, Thomas GP, Chen WY, Taft RJ, Nielsen LK, Enright AJ, Mattick JS, Dinger ME. Quantitative gene profiling of long noncoding RNAs with targeted RNA sequencing. *Nat Methods*. 2015;**12**(4):339–342.
84. Schilling T, Pecherstorfer M, Blind E, Leidig G, Ziegler R, Raue F. Parathyroid hormone-related protein (PTHrP) does not regulate 1,25-dihydroxyvitamin D serum levels in hypercalcemia of malignancy. *J Clin Endocrinol Metab*. 1993;**76**(3):801–803.
85. Nakayama K, Fukumoto S, Takeda S, Takeuchi Y, Ishikawa T, Miura M, Hata K, Hane M, Tamura Y, Tanaka Y, Kitaoka M, Obara T, Ogata E, Matsumoto T. Differences in bone and vitamin D metabolism between primary hyperparathyroidism and malignancy-associated hypercalcemia. *J Clin Endocrinol Metab*. 1996;**81**(2):607–611.
86. Shivnani SB, Shelton JM, Richardson JA, Maalouf NM. Hypercalcemia of malignancy with simultaneous elevation in serum parathyroid hormone-related peptide and 1,25-dihydroxyvitamin D in a patient with metastatic renal cell carcinoma. *Endocr Pract*. 2009;**15**(3):234–239.
87. Corbetta S, Mantovani G, Lania A, Borgato S, Vicentini L, Beretta E, Faglia G, Di Blasio AM, Spada A. Calcium-sensing receptor expression and signalling in human parathyroid adenomas and primary hyperplasia. *Clin Endocrinol (Oxf)*. 2000;**52**(3):339–348.